Article:
Drayton, Alexander, Li, Kezheng, Simmons, Mattrew et al. (2 more authors) (2020) Performance limitations of resonant refractive index sensors with low-cost components. Optics Express. 400236. pp. 32239-32248. ISSN: 1094-4087

https://doi.org/10.1364/OE.400236

Research Article | Vol. 28, No. 22 / 26 October 2020 / Optics Express 32239
Optics EXPRESS

Performance limitations of resonant refractive index sensors with low-cost components

ALEXANDER DRAYTON,[1,*] KEZHENG LI,[1] MATTHEW SIMMONS,[2] CHRISTOPHER REARDON,[1] AND THOMAS F KRAUSS[1]

[1]Department of Physics, University of York, Heslington, York, YO10 5DD, UK
[2]Department of Electronic Engineering, University of York, Heslington, York, YO10 5DD, UK
[*]alex.drayton@york.ac.uk

Abstract: Resonant biosensors are attractive for diagnostics because they can detect clinically relevant biomarkers with high sensitivity and in a label-free fashion. Most of the current solutions determine their detection limits in a highly stabilised laboratory environment, which does, however, not apply to real point-of-care applications. Here, we consider the more realistic scenario of low-cost components and an unstabilised environment and consider the related design implications. We find that sensors with lower quality-factor resonances are more fault tolerant, that a filtered LED lightsource is advantageous compared to a diode laser, and that a CMOS camera is preferable to a CCD camera for detection. We exemplify these findings with a guided mode resonance sensor and experimentally determine a limit of detection of $5.8 \pm 1.7 \times 10^{-5}$ refractive index units (RIU), which is backed up by a model identifying the various noise sources. Our findings will inform the design of high performance, low cost biosensors capable of operating in a real-world environment.

1. Introduction

Optical refractive index sensors are attractive because of their high performance and their ability to provide real-time results with minimal sample preparation. They do not require fluorescent or other labelling, which makes them highly suitable for point-of-care applications. Examples include surface plasmon resonance (SPR) [1–3], guided-mode resonance (GMR) [4–8], microring resonator [9–11] and interferometric sensors [12–15]. Each modality utilises the principle of a confined mode, a fraction of which interacts with the sample. For biomolecular detection applications, the specific capture of biomolecules at the sensor surface then results in a local change in refractive index, which produces the sensing signal that enables quantification of the biomolecules in the sample.

Several very high-performance refractive index sensors have already been described in the literature with limits of detection (LOD) down to the 10^{-9} refractive index unit (RIU) regime [2,16–19]. Several papers have also discussed the fundamental limitations of high Quality (Q) factor resonant sensors [19,20]. The main issue with these studies is that they assume a highly stabilised laboratory environment, very narrow linewidth lasers and/or high-resolution spectrometers. Unfortunately, these conditions cannot be met in a point-of-care or a resource-limited environment; for example, thermal fluctuations increase the noise of the system and low-cost lasers that are suitable for handheld devices do not exhibit the linewidth and stability of laboratory grade lasers. Therefore, a study is required to understand the limitations of refractive index sensors in a low-cost environment and to identify the best strategy, e.g. whether to use a resonance with a low or a high Q factor. We note that some work has already been done in this direction and a number of point-of-care (POC) devices based on photonic structures have previously been presented [14,21–26], but typically, only particular achievements are reported.

#400236 https://doi.org/10.1364/OE.400236
Journal © 2020 Received 16 Jun 2020; revised 1 Sep 2020; accepted 1 Sep 2020; published 12 Oct 2020

Optics EXPRESS

Here, we consider the trade-offs and key factors of the entire sensor system in order to evaluate the optimum solution for a low-cost POC device.

2. Sensor configuration

The key questions considered were the choice of lightsource (laser vs LED), which is directly connected to the Q-factor of the photonic resonance; the choice of the manufacturing method of the sensor (electron-beam lithography vs nanoimprint lithography) and the choice of sensor/detector (CCD vs CMOS camera).

2.1. Low-Q vs. high-Q resonant system

We started with the question of whether to use an optical resonance with a low or a high Q-factor. White and Fan [27] and Hu et al. [19] both conclude that high-Q factor resonances result in the highest sensor performance, up to Q-values of $Q \approx 10^5$. This upper limit typically arises from the intensity and wavelength noise of the laser source. Unfortunately, low-cost lasers tend to exhibit much higher noise values. For example, in Fig. 1(a), we show the wavelength noise of a Fabry-Perot laser (Roithner LaserTechnik GmbH - QL85D6SA), where we observe mode-hopping, resulting in wavelength changes of 1-2 nm for a period of 90 minutes; the intensity noise is shown in Fig. 1(b), exhibiting significant relative intensity noise and a drift ≈30% even when driven by a stable power source, i.e. a battery. Vertical cavity lasers typically avoid mode-hopping, but they are prone to changes in polarisation and have a broader linewidth (typ. $\Delta\lambda \approx 0.5$nm-1nm). It is also worth noting that the laser diode required an ND filter of 0.7 OD to reduce the power level and bring it closer to that of the filtered RCLED. Therefore, neither a simple Fabry-Perot nor a vertical cavity laser is suitable for use with a high-Q resonance. Moreover, the mass production of laser diodes means they have an operating wavelength tolerance up to $\Delta\lambda_{tol} \approx 10$ nm, which makes it extremely difficult to match the resonance of the sensor to the wavelength of the laser. These considerations alone are sufficient to conclude that a high-Q system is not suitable for a point-of-care solution operating with low-cost lasers.

We therefore propose to use an LED (in particular a resonant cavity LED (RCLED), because of its higher directionality and spectral density [28–30]), in combination with a wavelength filter. The filter adds cost, but given its small size, this is only a minor addition, and the centre wavelength of a filter is much better defined than that of a laser. We note that the filtered LED has lower intensity noise than the laser (Fig. 1(b)), and, as discussed in the context of Fig. 4 below, speckle noise is also avoided. Furthermore, we note that thermal wavelength drift is smaller for the filtered RCLED than for a laser, which is particularly important for point-of-care applications that operate in a temperature-variable environment; for example, the thermal drift for a VCSEL is typically $\Delta\lambda/DT \approx 0.06$ nm/K, while the filter drift (Andover Corp.) is specified as $\Delta\lambda/DT \approx 0.02$ nm/K, so the filtered RCLED offers higher wavelength stability than a laser. With these considerations in mind, it is important to consider what Q-factor to use. Any readout of a resonant system is a convolution of the resonance linewidth and the source linewidth. As there are wavelength limitations of 1-3 nm for typical low-cost sources (e.g. Figures 1(a) and 1(d)), high Q modalities such as ring resonators are not suitable and medium Q realisations are preferable instead. We therefore choose a guided-mode resonance (GMR) sensor with a linewidth of 3.4 nm (Q=190 at 650 nm operation wavelength) close to this limit in order to exemplify such a medium Q modality. The GMR sensor is also compatible with the reduced spectral density and the lack of coherence of the RCLED vs the laser light source, as it is excited with a collimated beam and does not require coupling into a narrow waveguide. A further consideration is the thermal noise of the system, which is often dealt with via a reference channel or by engineering the thermo-optic coefficient of the waveguide/resonant structure [31]; in this context, it has already been recognised [27] that low Q sensors are less susceptible to thermal stability issues. Regarding the use of a reference channel, its ability to compensate temperature fluctuations is limited by

Optics EXPRESS

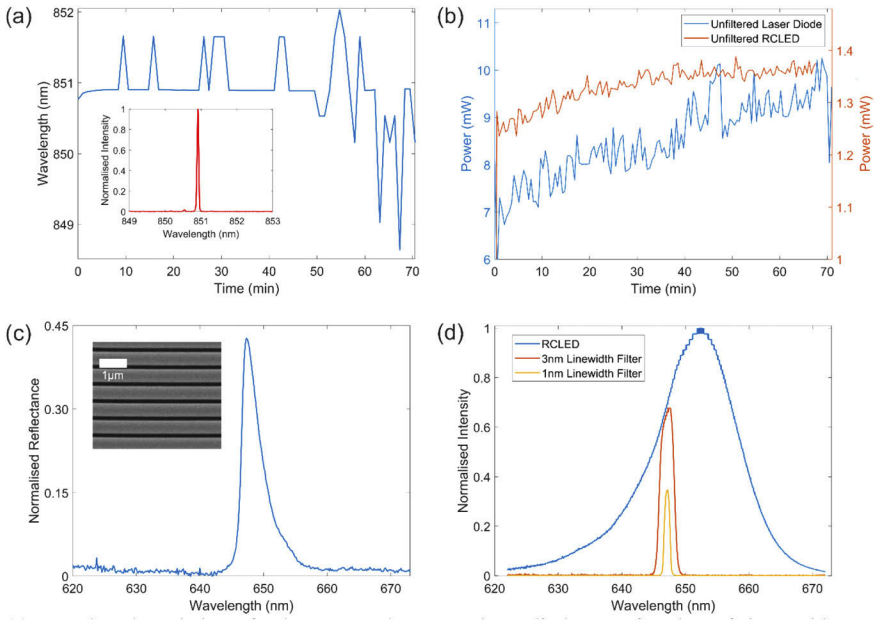

Fig. 1. (a) Wavelength variation of a low-cost Fabry Perot laser diode as a function of time, with an example spectrum. (b) Intensity variation (normalised to peak value) of a laser diode and a resonant cavity LED as a function of time, both powered by a battery. (c) Guided mode resonance (GMR) with a Q factor = 190 normalised to a high-quality mirror. (d) Spectrum of a resonant cavity LED with a 3 nm and 1 nm linewidth filter, both at 647 nm.

the spatial separation between channels [19]. While it is difficult to provide hard numbers for the thermal-fluctuation limited performance of POC sensors, our interpretation of the literature is that the lower bound for the limit of detection in a non-thermally stabilised system is in the 10^{-5}–10^{-6} RIU range [19,20,27,31]. As we will show, this level of performance can be achieved with a low Q system and with filtered LED illumination.

The next consideration is the spectral analysis of the signal, which either requires the lightsource to be tunable or a high-resolution spectrometer to be used. One possible solution is an on-chip arrayed waveguide grating [32]. As an alternative, we have developed the chirped GMR modality [33] which translates spectral information into the spatial domain, which is an imaging method that has the advantage of combining both the sensing and spectrometer function within the same element. Using imaging as the transduction method results in the uniformity of the illumination becoming an important factor, hence our choice of a non-coherent light source which avoids the noise associated with speckle is advantageous; this is discussed further in the context of Fig. 4 and 5. The complete system then consists of the sensor chip which is illuminated with the collimated, filtered RCLED and imaged onto the camera, with a beamsplitter combining the two beam paths (Fig. 2). Given the size of the sensor chip of 1mm and the size of a typical camera sensor of 2 mm, we arrange the imaging lens to provide a 2:1 magnification.

2.2. Sensor chip fabrication: electron beam lithography vs. nanoimprint

For the purpose of research, we use electron-beam lithography to define the sensor chip, which is clearly not low-cost nor scalable. We note, however, that our sensor is compatible with CMOS technology, so could be manufactured accordingly. An alternative low-cost, scalable method is nanoimprint lithography (NIL), which we demonstrate here. In fact, nanoimprinted GMR sensor chips have already been demonstrated by Cunningham et al. [34–36]. Here, we have

Optics EXPRESS

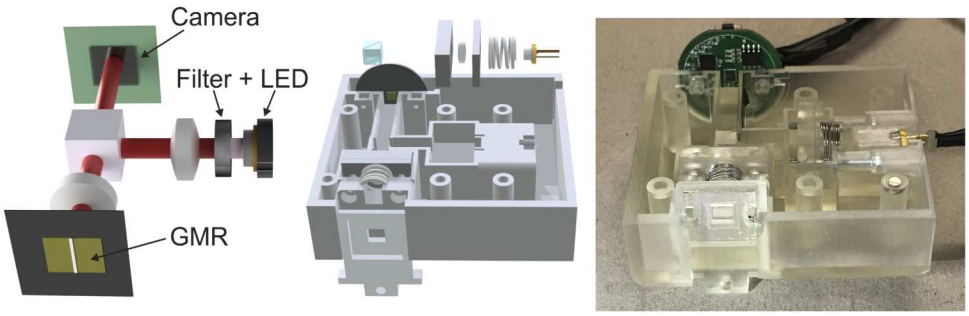

Fig. 2. Illustration of the beam path, CAD schematic and 3D printed sensor system on the basis of a chirped GMR sensor.

tested NIL as a method of producing GMRs of the same design as those made by electron beam lithography. Figure 3 shows a comparison and highlights that the linewidth and dynamic range of the resonance curves are very similar. Figure 3(a) shows the speckle noise from a coherent light source while Fig. 3(b) shows that an RCLED is only slightly broader than the filtered Halogen laboratory source used in Figs. 3(c) and 3(d). We have tested 20 samples of nanoimprinted GMRs, all of which show slight variations, and Fig. 3(e) provides a representative example. In order to create the resonance curves in Fig. 3(e), we average the intensity of the pixel across the resonant bars of Figs. 3(c) and (d), respectively, to produce 1D line plots. The line plot is then fitted with a Fano lineshape [37], and the maximum of the Fano curve is tracked as a function of refractive index.

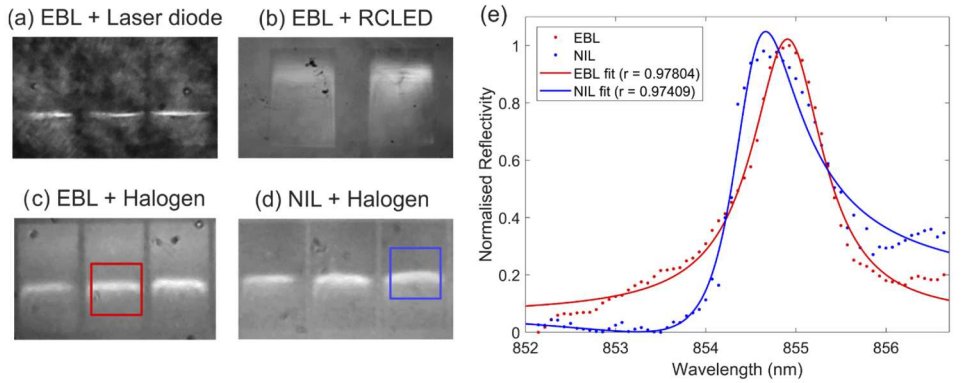

Fig. 3. (a) –(d)Chirped GMR sensors produced via Electron beam lithography (EBL) and Nanoimprint Lithography (NIL) illuminated with various sources. The RCLED is filtered with a 1 nm Linewidth filter. The Halogen source is filtered with a Monochromator. (e) Normalised reflectivity of (c) and (d) with FWHM of 0.928 nm and 1.071 nm for the EBL and NIL samples respectively.

2.3. Choice of camera sensor

There are two options for the camera sensor, i.e. charge-coupled device (CCD) or a complementary metal-oxide-semiconductor (CMOS) sensor [38,39]. Both types are available at low-cost and a CCD appears the more obvious choice given the technology's maturity. On the other hand, smartphone technology has driven down the price of CMOS sensors and driven up their technological development. Operationally, CCDs use a shift register to move the carriers

Optics EXPRESS

generated at each pixel and have a single amplifier per row of pixels. Because charges are shifted repeatedly during readout, CCD sensors experience temporal noise [40]. Temporal noise is an effect not usually noticed by the human eye, but as it is an inherently time-dependent property, it impacts on the sensor performance. CCDs can also suffer from smear where excess charge 'bleeds' into adjacent pixels. In contrast, CMOS sensors have individual amplifiers per pixel, which means that CMOS sensors experience neither temporal noise nor bleeding, however each pixel may experience different offsets and sensitivity curves. These variations lead to fixed pattern noise and gain noise; since these do not change over time, they can be compensated and most manufacturers design driving circuits accordingly, although not necessarily in low-cost devices. Another parameter is the dynamic range, which tends to be higher for a CCD than for a CMOS sensors. In terms of fill-factor, CCDs are able to reach near 100%, while most CMOS sensors cannot, due to the driving electronics, which reduces their signal to noise ratio.

Given this wide parameter-space, it is difficult to make the optimum choice, so it is best determined by comparison and experimental measurement, such as the protocol outlined in [41]. In the system test in section 3.2, we show that the CMOS camera is superior to the CCD, partly because it can reach smaller pixel sizes but also because of its lower noise floor. Pixel size matters because a larger number of pixels provides more information and affords a more accurate fit to the Fano curve (Fig. 3(e)). While the number of pixels involved in the curve-fitting could be increased by increasing the magnification of the optical system, this would also increase the required accuracy of placing the sensor chip in the imaging plane. Instead, a camera with a smaller pixel size allows for a lower magnification and higher tolerance, which is the better solution in the context of this study.

3. Results

3.1. Experimental limit of detection

For the systems test, we used a GMR written by electron-beam lithography, illuminated by a RCLED with a 1 nm line filter and a CMOS camera with 2.2 μm pixel size. To achieve the maximum intensity of the resonance on the camera, an integration time of 105ms was used. The acquisition rate was approximately 1 image every 3 seconds as biological binding happens on a much slower time scale. Given the simplicity and high throughput of the optical path, the spectrally filtered LED provides sufficient signal to produce a high dynamic range image on the CMOS camera. Glucose solutions of different concentrations and thus different refractive indices were used to measure the sensitivity (Fig. 3(b)) and the system noise (Fig. 3(a)) with the limit of detection (LOD) given by dividing the 3σ noise value by the sensitivity. The results are shown in Fig. 4, and the LOD from a total of 12 measurements was found to be $5.8 \pm 1.7 \times 10^{-5}$ RIU. This value is in good agreement with other refractive index sensors in laboratory setups [42], and typically allows the detection of protein concentrations in the low ng/ml or high pg/ml range [43].

3.2. Simulation of performance

Finally, we simulated the impact of the various components in order to understand their contribution to the overall noise value. The starting point was an ideal Fano resonance curve simulated with rigorous wave couple analysis (RCWA), using the open source software S4 [44]. Various noise profiles were then superimposed onto this ideal Fano curve. Experimental measurements of the different sources of noise, for example the random variations of speckle noise from a laser diode are illustrated in Fig. 3(a). The camera noise was obtained by measuring the variation of pixel values for constant illumination. The intensity noise of the illumination sources was obtained from the data shown in Fig. 1(b) and their linewidth was simulated using a Gaussian lineshape. The normalised standard deviations of the main contributions to noise used in this model are shown in Table 1. The pixel size was simulated by changing the sampling rate

Optics EXPRESS

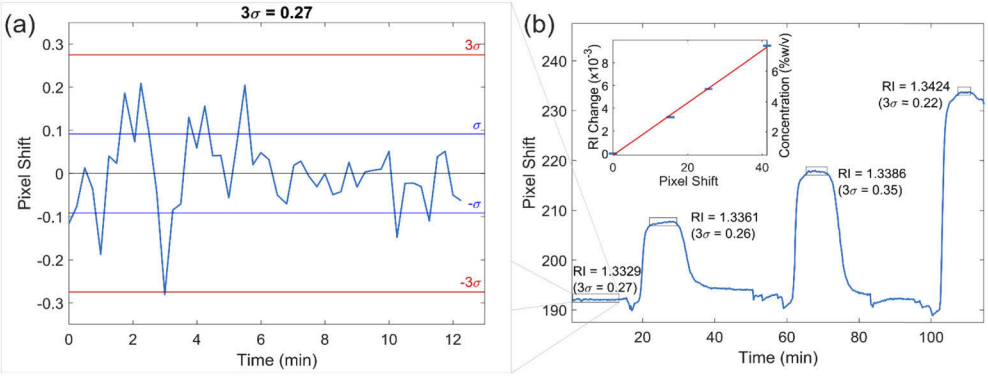

Fig. 4. Experimental determination of the limit of detection of the device using a GMR sensor shown in Fig 2. (a) The 3σ noise value when measuring fixed refractive index value (DI water). As we sample every 15s and the time window is 8-12 minutes, we typically use 30-50 data points to determine the standard deviation which is statistically significant with a confidence of better than 95%. (b) sensitivities from varying concentrations of glucose solution providing a limit of detection of $5.8 \pm 1.7 \times 10^{-5}$RIU.

of the ideal curve to represent the number of pixels used to image a resonance. The speckle noise was obtained experimentally, in a similar way as the camera noise, by illuminating a fixed image with a laser and measuring the intensity. The wavelength noise shown in Fig. 1(a) was discounted as it would have been by far the largest source of noise and would have overly dominated the study. Due to the minimal difference between GMRs written by EBL and NIL, highlighted in Fig. 4, this comparison was not included in the model either.

Table 1. Noise contributions of the main elements to the system performance expressed as normalised standard deviations as shown in Fig. 5. These numbers confirm the observation that once speckle noise is removed, camera noise dominates over intensity noise.

Noise Component per pixel area affected	CCD (3.2 µm pixel size)	CMOS (2.2 µm pixel size)
Pixel Noise	18×10^{-3}	5×10^{-3}
Laser Diode Intensity	0.8×10^{-3}	0.5×10^{-3}
Laser Diode Speckle	12×10^{-3}	8×10^{-3}
RCLED Intensity	0.2×10^{-3}	0.1×10^{-3}

The noisy data was then used to fit a Fano curve as described in section 2.2. Each condition was repeated 200 times to simulate measuring a fixed refractive index and to generate a 3σ value, similar to the data shown in Fig. 4(a). Each 3σ value was generated 20 times and averaged to remove random number generation noise from the model, which is essentially a Monte-Carlo simulation. The results of the model are shown in Fig. 5, with the figure splitting data into two separate data ranges for clarity. Figure 5 allows us to make several noteworthy observations. For a start, the disadvantage of the speckle noise of a coherent source outweighs its linewidth advantage. In order to assess the impact of the speckle noise alone, we included data that could be achieved with use of a de-speckler, such as a rotating diffuser disc [45], which would however increase system complexity. Interestingly, the result achieved with a 1 nm linewidth filter is essentially the same as that achieved with a de-speckled laser of 53.2 pm linewidth from Fig. 1(a). As the response of the system is a convolution of the resonance linewidth and the source linewidth, the broader of the two will dominate. Furthermore, and related to the choice of Q-factor of the resonance, a more detailed study shows that the 3σ value improves up to Q-values of 200-300, but then does not improve much further. This supports our choice of Q-factor of 190. Clearly, the

Optics EXPRESS

exact optimum depends on the particular parameters of each experiment, but this study suggests that a resonance with a moderate Q-factor of order 100-400 appears to be a good choice.

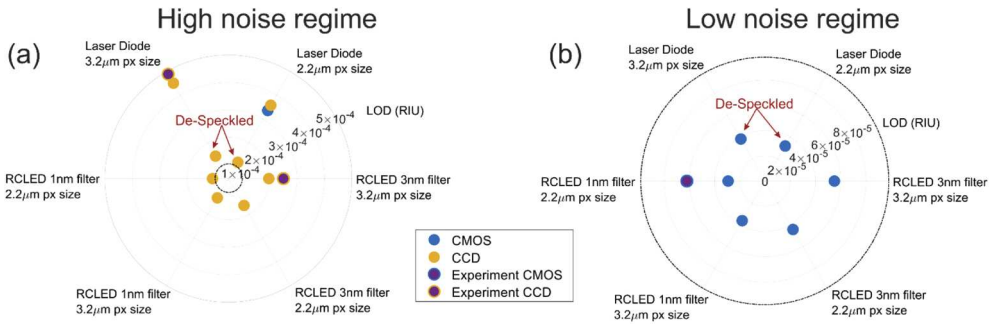

Fig. 5. A plot showing the data from a Monte Carlo simulation of noise added to a simulated GMR Spectrum compared to Experimental values. (a) Results greater than 1×10^{-4}RIU. (b) Results lower than 1×10^{-4}RIU. The dashed line shows where (b) sits in (a).

Another finding is that the noise from the camera had the largest effect for the two types of cameras we compared, so the CMOS camera was significantly better than the CCD; this is highlighted by the fact that almost all of the points in the high noise plot of Fig. 5(a)) are CCD, while they are CMOS in the low noise regime of Fig. 5(b); the pixel size then had a smaller effect, with smaller pixel size being slightly advantageous due to better sampling. The experimental values are slightly higher than the simulated ones but follow the same trend, which gives us confidence in the general conclusions we are able to draw.

4. Discussion and conclusion

We have presented some considerations for resonant refractive index sensors with low-cost components and have considered the impact of the various noise sources on the overall systems performance. Regarding cost, we estimate that the OEM cost of all the sensor components (Fig. 2) is of order 10 US$. We conclude that the light source is a key determining factor; while many previous studies have based their findings on a stabilised light source in a laboratory, we note that wavelength variations and wavelength noise of available low-cost sources precludes the use of a diode laser, and that in fact, a filtered LED is a better solution. Having reached this conclusion, the obvious consequence is to use a sensor with a low-to-medium Quality factor. Here, we use a guided mode resonance (GMR) sensor with a Q-factor of 190 at a wavelength of 650nm illuminated by a resonant cavity LED (RCLED) through a $\Delta\lambda$=1 nm filter. With the wavelength noise minimised by this approach, other noise sources then dominate, with the camera and the readout system making the next most significant contribution to the noise floor.

In terms of spectral readout, using a camera is a very cost-effective solution, based on the advances driven by smartphone technology, and we note that the camera readout is the dominant source of noise; this is especially true since the throughput of the optical system is very high such that the cameras operate well above their respective dark noise limits. By comparing a CCD and a CMOS camera, we have found that a CMOS camera gives superior results, both from its experimentally measured noise but also from its smaller pixel size that affords better sampling. Given that we use an imaging approach to extract the spectral information, using the filtered LED provides the added bonus of avoiding speckle noise, which is the dominant source of noise for a coherent light source. When comparing our results with others presented in the literature, it is clear that handheld low-cost systems usually use low Q resonances [4,14,22,25]; many also use broadband (LED) sources and camera sensors. The exception to this being the intensity based readout of a photonic crystal by Paulsen et al. [4], who use a photodetector instead of a

Optics EXPRESS

full camera sensor, which makes detection more susceptible to the intensity noise of the source; consequently they report a higher LOD in the low 10^{-3} RIU range. The difference between this intensity-based readout and the spectral readout of [14,22,25] is analogous to AM and FM encoding in communications, with AM being known to be more noisy; the cost of lower noise in FM is a higher bandwidth requirement, which is equivalent to the need for collecting more data for a spectral readout. The solution by Martens et al. [14] is interesting in this regard and probably the most highly performing low-cost sensor we have found. They use a Mach-Zehnder interferometer to provide a highly sensitive response, which is intrinsically an "AM" solution, but then feed it through a spectrometer to create "FM" data which elegantly mitigates the effect of intensity noise. With this configuration they are able to achieve a limit of detection of 6×10^{-6} RIU. However, the requirement of needing an expensive superluminescent diode because of the poor coupling efficiency into the circuit and the fact that silicon photonics circuits only reach low cost for very high volumes somewhat weakens the "low cost" argument for this modality.

The insights gained in this study have helped us to develop a low cost, high performance refractive index sensor based on the guided mode resonance (GMR) modality. The GMR is a low Q modality excited by a resonant cavity LED and we have achieved a refractive index limit of detection of $5.8 \pm 1.7\times10^{-5}$RIU. The system is limited by the noise of the camera as well as by the low Q nature of the sensing chip, however the low Q makes it more robust to general noise. The limit of detection we have measured is comparable to other, laboratory based systems that have measured biomarkers at clinically relevant concentrations, so we expect to also be able to detect proteins in the low ng/ml or pg/ml range. For example, Cetin et al. [46] have shown in laboratory measurements that plasmonic nanohole arrays with a refractive index limit of detection of 2×10^{-5}RIU can detect 700pg/ml of IgG; the same configuration later achieved 145pg/ml of vascular endothelial growth factor [47]. Luan et al. [48] have shown that with a limit of detection of 3.3×10^{-4}RIU, they can reach detection limits of 5.5ng/ml for biotin. Kenaan et al. [49] have demonstrated the detection of 10pg/ml for CRP with a stated LOD of 5.8×10^{-5}RIU for a GMR system in the laboratory. By having explained the contributions of the various elements to the overall system noise, we believe that such low detection limits are now also achievable with low-cost components.

Funding

Engineering and Physical Sciences Research Council (EP/P02324X/1, EP/P030017/1); Royal Society (WM150005).

Disclosures

The authors declare no conflicts of interest.

References

1. Z. Altintas, Y. Uludag, Y. Gurbuz, and I. E. Tothill, "Surface plasmon resonance based immunosensor for the detection of the cancer biomarker carcinoembryonic antigen," Talanta **86**, 377–383 (2011).
2. A. V. Kabashin, S. Patskovsky, and A. N. Grigorenko, "Phase and amplitude sensitivities in surface plasmon resonance bio and chemical sensing," Opt. Express **17**(23), 21191–21204 (2009).
3. . GE Healthcare white paper, "BiacoreTM Systems in Vaccine Development and Production" (GE Healthcare, 2010).
4. M. Paulsen, S. Jahns, and M. Gerken, "Intensity-based readout of resonant-waveguide grating biosensors: Systems and nanostructures," Photonic Nanostruct. **26**, 69–79 (2017).
5. A. Drayton, I. Barth, and T. F. Krauss, "Guided mode resonances and photonic crystals for biosensing and imaging," in *Semiconductors and Semimetals 100, Photonic Crystal Metasurface Optoelectronics* (2019), pp. 115–148.
6. S. S. Wang and R. Magnusson, "Theory and applications of guided-mode resonance filters," Appl. Opt. **32**(14), 2606–2613 (1993).
7. Y. Zhuo and B. T. Cunningham, "Label-free biosensor imaging on photonic crystal surfaces," Sensors **15**(9), 21613–21635 (2015).
8. B. T. Cunningham, P. Li, S. Schulz, B. Lin, C. Baird, J. Gerstenmaier, C. Genick, F. Wang, E. Fine, and L. Laing, "Label-free assays on the BIND system," J. Biomol. Screening **9**(6), 481–490 (2004).

Optics EXPRESS

9. E. Valera, W. W. Shia, and R. C. Bailey, "Development and validation of an immunosensor for monocyte chemotactic protein 1 using a silicon photonic microring resonator biosensing platform," Clin. Biochem. **49**(1-2), 121–126 (2016).
10. W. Bogaerts, P. de Heyn, T. van Vaerenbergh, K. de Vos, S. Kumar Selvaraja, T. Claes, P. Dumon, P. Bienstman, D. van Thourhout, and R. Baets, "Silicon microring resonators," Laser Photonics Rev. **6**(1), 47–73 (2012).
11. Genalyte white paper, "Novel Multiplex Measurement of Macromolecules Binding To A Solid Phase Using Photonic Microring Sensors" (Genalyte).
12. Y. Liang, M. Zhao, Z. Wu, and G. Morthier, "Bimodal Waveguide Interferometer RI Sensor Fabricated on Low-Cost Polymer Platform," IEEE Photonics J. **11**(2), 1–8 (2019).
13. J. C. Ramirez, L. M. Lechuga, L. H. Gabrielli, and H. E. Hernandez-Figueroa, "Study of a low-cost trimodal polymer waveguide for interferometric optical biosensors," Opt. Express **23**(9), 11985–11994 (2015).
14. D. Martens, P. Ramirez-Priego, M. S. Murib, A. A. Elamin, A. B. Gonzalez-Guerrero, M. Stehr, F. Jonas, B. Anton, N. Hlawatsch, P. Soetaert, R. Vos, A. Stassen, S. Severi, W. van Roy, R. Bockstaele, H. Becker, M. Singh, L. M. Lechuga, and P. Bienstman, "A low-cost integrated biosensing platform based on SiN nanophotonics for biomarker detection in urine," Anal. Methods **10**(25), 3066–3073 (2018).
15. "Antelope DX," https://www.antelope-dx.com.
16. K. Schmitt, B. Schirmer, C. Hoffmann, A. Brandenburg, and P. Meyrueis, "Interferometric biosensor based on planar optical waveguide sensor chips for label-free detection of surface bound bioreactions," Biosens. Bioelectron. **22**(11), 2591–2597 (2007).
17. A. Ymeti, J. Greve, P. v. Lambeck, R. Wijn, R. G. Heideman, and J. S. Kanger, "Drift correction in a multichannel integrated optical Young interferometer," Appl. Opt. **44**(17), 3409–3412 (2005).
18. S. Aikio, M. Hiltunen, P. Stenberg, and J. Hiltunen, "Drift compensation using a multichannel slot waveguide young interferometer," JEOS:RP **10**, 15053 (2015).
19. J. Hu, X. Sun, A. Agarwal, and L. C. Kimerling, "Design guidelines for optical resonator biochemical sensors," J. Opt. Soc. Am. B **26**(5), 1032–1041 (2009).
20. K. Saurav and N. le Thomas, "Probing the fundamental detection limit of photonic crystal cavities: erratum," Optica **4**(10), 1305 (2017).
21. S. Jahns, M. Bräu, B.-O. Meyer, T. Karrock, S. B. Gutekunst, L. Blohm, C. Selhuber-Unkel, R. Buhmann, Y. Nazirizadeh, and M. Gerken, "Handheld imaging photonic crystal biosensor for multiplexed, label-free protein detection," Biomed. Opt. Express **6**(10), 3724–3736 (2015).
22. D. Gallegos, K. D. Long, H. Yu, P. P. Clark, Y. Lin, S. George, P. Nath, and B. T. Cunningham, "Label-free biodetection using a smartphone," Lab Chip **13**(11), 2124 (2013).
23. A. B. González-Guerrero, J. Maldonado, S. Dante, D. Grajales, and L. M. Lechuga, "Direct and label-free detection of the human growth hormone in urine by an ultrasensitive bimodal waveguide biosensor," J. Biophotonics **10**(1), 61–67 (2017).
24. F. Yesilkoy, R. A. Terborg, J. Pello, A. A. Belushkin, Y. Jahani, V. Pruneri, and H. Altug, "Phase-sensitive plasmonic biosensor using a portable and large field-of-view interferometric microarray imager," Light: Sci. Appl. **7**(2), 17152 (2018).
25. N. Fabri-Faja, O. Calvo-Lozano, P. Dey, R. A. Terborg, M.-C. Estevez, A. Belushkin, F. Yesilköy, L. Duempelmann, H. Altug, V. Pruneri, and L. M. Lechuga, "Early Sepsis Diagnosis via Protein and miRNA Biomarkers using a novel Point-of-Care Photonic Biosensor," Anal. Chim. Acta **1077**, 232–242 (2019).
26. R. A. Terborg, L. Duempelmann, J. Pello, A. Noyan, F. Yesilkoy, A. A. Belushkin, Y. Jahani, N. Fabri-Faja, P. Dey, O. Calvo-Lozano, M.-C. Estevez, A. Fàbrega, J. J. González-López, L. M. Lechuga, H. Altug, and V. Pruneri, "Lens-Free Interferometric Microscope for Point-of-Care Label-Free Detection of Sepsis Biomarkers," in *Frontiers in Optics + Laser Science APS/DLS* (OSA Technical Digest (Optical Society of America, 2019), 2019), p. FM3F.6.
27. I. M. White and X. Fan, "On the performance quantification of resonant refractive index sensors," Opt. Express **16**(2), 1020–1028 (2008).
28. R. G. Baets, D. Delbeke, R. Bockstaele, and P. Bienstman, "Resonant-Cavity Light-Emitting Diodes: a review," in *Light-Emitting Diodes: Research, Manufacturing, and Applications VII* (International Society for Optics and Photonics, 2003), 4996, pp. 74–86.
29. X. Buet, E. Daran, D. Belharet, F. Lozes-Dupuy, A. Monmayrant, and O. Gauthier-Lafaye, "High angular tolerance and reflectivity with narrow bandwidth cavity-resonator-integrated guided-mode resonance filter," Opt. Express **20**(8), 9322 (2012).
30. H. de Neve, J. Blondelle, R. Baets, P. Demeester, P. van Daele, and G. Borghs, *Resonant Cavity LED's. In Microcavities and Photonic Bandgaps: Physics and Applications* (Springer, 1996).
31. X. Fan, I. M. White, S. I. Shopova, H. Zhu, J. D. Suter, and Y. Sun, "Sensitive optical biosensors for unlabeled targets: A review," Anal. Chim. Acta **620**(1-2), 8–26 (2008).
32. D. Martens, A. Z. Subramanian, S. Pathak, M. Vanslembrouck, P. Bienstman, W. Bogaerts, and R. G. Baets, "Compact silicon nitride arrayed waveguide gratings for very near-infrared wavelengths," IEEE Photonics Technol. Lett. **27**(2), 137–140 (2015).
33. G. J. Triggs, Y. Wang, C. P. Reardon, M. Fischer, G. J. O. Evans, and T. F. Krauss, "Chirped guided-mode resonance biosensor," Optica **4**(2), 229–234 (2017).
34. W. Chen, K. D. Long, H. Yu, Y. Tan, J. S. Choi, B. A. Harley, and B. T. Cunningham, "Enhanced live cell imaging via photonic crystal enhanced fluorescence microscopy," Analyst **139**(22), 5954–5963 (2014).

Optics EXPRESS

35. C. J. Choi, I. D. Block, B. Bole, D. Dralle, and B. T. Cunningham, "Label-free photonic crystal biosensor integrated microfluidic chip for determination of kinetic reaction rate constants," IEEE Sens. J. **9**(12), 1697–1704 (2009).
36. M. Lu, S. J. Park, B. T. Cunningham, and J. G. Eden, "Microcavity plasma devices and arrays fabricated by plastic-based replica molding," J. Microelectromech. Syst. **16**(6), 1397–1402 (2007).
37. M. F. Limonov, M. v. Rybin, A. N. Poddubny, and Y. S. Kivshar, "Fano resonances in photonics," Nat. Photonics **11**(9), 543–554 (2017).
38. M. Bigas, E. Cabruja, J. Forest, and J. Salvi, "Review of CMOS image sensors," Microelectron. J. **37**(5), 433–451 (2006).
39. B. Kisacanin, S. S. Bhattacharyya, and S. Chai, *Embedded Computer Vision* (Springer Science & Business Media, 2008).
40. H. Tian, B. Fowler, and A. el Gamal, "Analysis of Temporal Noise in CMOS Photodiode Active Pixel Sensor," IEEE J. Solid-State Circuits **36**(1), 92–101 (2001).
41. . Teledyne Photometrics white paper, Technical Note: Camera Test Protocol (Teledyne Photometrics, 2019).
42. M. Soler, O. Calvo-Lozano, M.-C. Estevez, and L. M. Lechuga, "Nanophotonic Biosensors Driving Personalized Medicine," Opt. Photonics News **31**(4), 24–31 (2020).
43. G. Pitruzzello and T. F. Krauss, "Photonic crystal resonances for sensing and imaging," J. Opt. **20**(7), 073004 (2018).
44. V. Liu and S. Fan, "S4: A free electromagnetic solver for layered periodic structures," Comput. Phys. Commun. **183**(10), 2233–2244 (2012).
45. T. Stangner, H. Zhang, T. Dahlberg, K. Wiklund, and M. Andersson, "Step-by-step guide to reduce spatial coherence of laser light using a rotating ground glass diffuser," Appl. Opt. **56**(19), 5427–5435 (2017).
46. A. E. Cetin, D. Etezadi, B. C. Galarreta, M. P. Busson, Y. Eksioglu, and H. Altug, "Plasmonic Nanohole Arrays on a Robust Hybrid Substrate for Highly Sensitive Label-Free Biosensing," ACS Photonics **2**(8), 1167–1174 (2015).
47. X. Li, M. Soler, C. I. Özdemir, A. Belushkin, F. Yesilköy, and H. Altug, "Plasmonic nanohole array biosensor for label-free and real-time analysis of live cell secretion," Lab Chip **17**(13), 2208–2217 (2017).
48. E. Luan, H. Yun, M. Ma, D. M. Ratner, K. C. Cheung, and L. Chrostowski, "Label-free biosensing with a multi-box sub-wavelength phase-shifted Bragg grating waveguide," Biomed. Opt. Express **10**(9), 4825–4838 (2019).
49. A. Kenaan, K. Li, I. Barth, S. Johnson, J. Song, and T. F. Krauss, "Guided mode resonance sensor for the parallel detection of multiple protein biomarkers in human urine with high sensitivity," Biosens. Bioelectron. **153**, 112047 (2020).